RESEARCH ARTICLE | JULY 11 2023

An adjoint-based drag reduction technique for unsteady flows

Carlos J. Ruiz-Sánchez ; Alejandro Martínez-Cava ; Miguel Chávez-Módena ; Eusebio Valero

Physics of Fluids 35, 073603 (2023)
https://doi.org/10.1063/5.0153892

Physics of Fluids ARTICLE pubs.aip.org/aip/pof

An adjoint-based drag reduction technique for unsteady flows

Cite as: Phys. Fluids **35**, 073603 (2023); doi: 10.1063/5.0153892
Submitted: 12 April 2023 · Accepted: 22 June 2023 ·
Published Online: 11 July 2023

Carlos J. Ruiz-Sánchez,[a] Alejandro Martínez-Cava,[b] Miguel Chávez-Módena,[c] and Eusebio Valero[c]

AFFILIATIONS

Universidad Politécnica de Madrid, Plaza Cardenal Cisneros, 3, E-28040 Madrid, Spain

[a]**Author to whom correspondence should be addressed:** carlosjesus.ruiz@upm.es
[b]**Also at:** Instituto Universitario "Ignacio Da Riva" (IDR/UPM), Universidad Politécnica de Madrid, Plaza Cardenal Cisneros, 3, E-28040 Madrid, Spain.
[c]**Also at:** CCS-UPM-Center for Computational Simulation, Universidad Politécnica de Madrid, Boadilla del Monte, E-28660 Madrid, Spain.

ABSTRACT

A framework based on a continuous adjoint-based analysis of steady and unsteady flows to predict and control the drag force due to surface morphing is presented. By establishing a relation between perturbations in the body shape and in the boundary condition on a certain geometry, we derive an analytical expression of the sensitivity to changes in the geometry of the body and its relation to the sensitivity to the perturbation of the boundary conditions. The methodology is evaluated on the incompressible flow around a cylinder for steady and unsteady flows. A reduction of the drag coefficient was obtained and investigated by several surface deformations, conducted in the direction of the sensitivity vector field obtained by solving the derived adjoint problem. In unsteady flows, the sensitivity field is computed by integrating the unsteady adjoint problem backward in time from the unsteady flow solution. Two different types of deformations based on the calculated sensitivity were applied: time-averaged deformation and time-dependent. Attempting the latter, a deformation at each time step, did not yield the same satisfactory results as the time-averaged in terms of expected drag reduction. We provide a theoretical reasoning for the difference between both methodologies, together with an insight into the physics of the sensitivity vector field distribution relating it to the drag force sources.

I. INTRODUCTION

Bodies immersed in a fluid flow experience a natural resistance in the direction of the fluid motion, the drag force. In bodies surrounded by incompressible flow, the drag force is caused by a combination of viscous and pressure forces, one of which may dominate over the other depending on how streamlined the body is shaped. The drag being proportional to the flow velocity, a common hydro or aerodynamic problem, is based on its reduction employing passive or active methodologies.[1] Passive methods generally involve modification of body shape,[2] while active methodologies rely on the flow control field, introduced as boundary layer actuation, among other techniques.[3–5] The magnitude of the drag forces can be influenced by several variables, from the flow conditions to a large set of geometrical parameters. Its minimization, therefore, faces a complex problem, where several inputs condition a specific output. In this regard, the use of adjoint methodologies presents a mathematical advantage over different approaches.[6] The use of the adjoint method in the optimization theory goes back for several decades.[7] The first time adjoint equations were used in the fluid mechanics design was in 1970 by Pironneau,[8] but it was not until 1988 with the help of Jameson[9,10] that the first applications were introduced in the field of computational fluid dynamics (CFD). From this point on, optimization algorithms began to be coupled with CFD solvers, with important contributions such as those made by Huffman *et al.*[11] or Elliott and Peraire.[12] For an exhaustive review of these early algorithms, the reader is referred to Newman *et al.*,[13] and for a first glance at this field, the work of Giles and Pierce[14] can be consulted. More recent contributions on the aim of drag reduction employing an adjoint mathematical approach directly address the problem through active flow control[15] or body geometry modifications,[16] targeting the minimization of the different drag sources. The former approach may be introduced as changes in the final shape of the rigid body or employing a temporal local surface morphing to alter the shape of the body toward optimal configurations depending on the performance point.[17] Surface morphing may be

exploited in aerodynamic performance,[18] and optimal directions for the local and temporal surface modification are then of great interest for the application of these novel methodologies for drag reduction.

Within the methodology of the adjoint method, a distinction must be made between continuous and discrete methods. In the discrete method, the equations are first discretized and then differentiated, to recover the associated adjoint and derivative systems. On the other hand, with the continuous approach, one obtains the adjoint and sensitivity equations directly from the constraints, like governing equations or the subset where we are looking for them, and the initial and boundary conditions with respect to the control variables. Then, these equations are adequately discretized and solved.

The effect caused by modifications of the surface body on drag forces has been widely explored, with recent contributions based on the application of a discrete adjoint approach.[16,19–23] However, these methods have limitations.[24]

In terms of application of continuous adjoint equations to unsteady flows, there are different studies that focus on changes of body geometries based on certain parameters,[25] such as parametric optimization,[26] RANS (Reynolds-averaged Navier–Stokes) equations within the field of aerospace engineering,[27] and biomedicine applications.[28] Nevertheless, there is still no generalized mathematical framework to address different problems.

Our study introduces a novel contribution by successfully applying the adjoint method to investigate the sensitivity to geometry changes in unsteady flows. This represents a significant advancement in the field of sensitivity analysis, as previous approaches have focused primarily on steady flows. By utilizing the adjoint method, renowned for its accuracy and efficiency in optimization, we have unlocked new possibilities to assess the impact of geometry modifications on dynamic fluid systems. Based on a continuous adjoint method, analytical expressions are derived for the calculation of the drag force sensitivities with respect to changes on the body geometry. This analytical approximation allows us to extract physical information as a function of the adjoint and original variables, giving an interpretation of the different terms of the deduced mathematical expressions, valid for both steady and unsteady flows and any geometry. Moreover, this novel approach allows consideration of non-uniform boundary conditions on the body of interest, as the usual non-zero velocity distribution used on the wall boundary condition for viscous flows is treated here as a parameter function.

Through the adjoint approach presented here, a time-dependent drag sensitivity function is recovered, which contains the optimal distribution of surface modifications to be applied toward drag reduction at every time step. We examine this sensitivity function from two points of view. First, a constant deformation calculated as the time average of the sensitivity function is enforced. Next, it is compared to a time-dependent surface morphing that deforms the body at each temporal iteration. As will be shown, a constant deformation performs better in terms of drag reduction than a time-dependent surface morphing. This is in line with the results of Meliga *et al.*,[29] who obtained similar results for a time-dependent boundary layer actuation. Here, a mathematical analysis is presented to explain this effect.

This paper is organized as follows.The theoretical framework is described in Sec. II, where a physical interpretation of the present formulation is included, followed by a description of the numerical methods in Sec. III. Next, a validation is carried out for steady and unsteady flows, for Reynolds numbers of $\mathrm{Re} = 40$ and $\mathrm{Re} = 100$. The drag force sensitivity is evaluated with respect to the introduction of an external force on the flow in the vicinity of the body of interest, and to modifications in the body boundary condition, namely, an implementation of a suction-blowing surface distribution. Afterward, the drag sensitivity to body morphing in unsteady flows is presented for a two-dimensional cylinder flow in Sec. IV. Finally, in Sec. V, we present the main conclusions of the study.

II. THEORETICAL FRAMEWORK

The goal of an optimization problem is to find the state of the system, $\mathbf{q}$, that minimizes or maximizes a scalar, the cost function $\mathscr{J} := \mathscr{J}(\mathbf{q}, \mathbf{g})$. We assume that $\mathscr{J}$ belongs to the C^1 class, with a particular value of $\mathbf{q}$ that cancels the gradient $\mathrm{d}J/\mathrm{d}\mathbf{q}$. In most cases, is almost impossible to find $\mathbf{q}$ that satisfies the condition and it is easier to act on some parameters of the design of the problem, $\mathbf{q}$.

To calculate the sensitivity of an unsteady cost function subjected to the aforementioned equations of state, with respect to a single parameter (or set of parameters), $\nabla_{\mathbf{g}}\mathscr{J}$, we introduce the Lagrangian functional as

$$\mathscr{L}(\mathbf{q}, \mathbf{g}, \lambda) = \mathscr{J} - \frac{1}{T}\int_0^T \langle \lambda, \mathbf{F}(\mathbf{q}, \mathbf{g}, t)\rangle \mathrm{d}t, \tag{1}$$

where λ is the adjoint variable, $(0, T)$ is the temporal window considered, and $\langle \cdot, \cdot \rangle$ is an L^2 inner product of the vector space to which belongs $\mathbf{q}$. Hence, a variation of the Lagrangian follows the following expression:

$$\delta\mathscr{L} = \frac{\partial \mathscr{L}}{\partial \mathbf{q}}\delta\mathbf{q} + \frac{\partial \mathscr{L}}{\partial \mathbf{g}}\delta\mathbf{g} + \frac{\partial \mathscr{L}}{\partial \lambda}\delta\lambda. \tag{2}$$

The extreme conditions are then enforced, since the Lagrangian reaches an extreme if $\delta\mathscr{L} = 0$ for all variations, imposing the following conditions on the derivatives:

$$\frac{\partial \mathscr{L}}{\partial \mathbf{q}} = \mathbf{0}, \tag{3}$$

$$\frac{\partial \mathscr{L}}{\partial \mathbf{g}} = \mathbf{0}, \tag{4}$$

$$\frac{\partial \mathscr{L}}{\partial \lambda} = \mathbf{0}. \tag{5}$$

Developing these derivatives from Eq. (1), we recover the optimization system

$$\nabla_{\mathbf{q}}\mathscr{L} := \frac{\partial \mathscr{L}}{\partial \mathbf{q}} = \frac{1}{T}\int_0^T \frac{\partial \mathbf{F}^*}{\partial \mathbf{q}}\lambda \mathrm{d}t - \frac{\partial \mathscr{J}}{\partial \mathbf{q}} = \mathbf{0}, \tag{6}$$

$$\nabla_{\mathbf{g}}\mathscr{L} := \frac{\partial \mathscr{L}}{\partial \mathbf{g}} = \frac{1}{T}\int_0^T \frac{\partial \mathbf{F}^*}{\partial \mathbf{g}}\lambda \mathrm{d}t - \frac{\partial \mathscr{J}}{\partial \mathbf{g}} = \mathbf{0}, \tag{7}$$

$$\nabla_{\lambda}\mathscr{L} := \frac{\partial \mathscr{L}}{\partial \lambda} = -\mathbf{F} = \mathbf{0}. \tag{8}$$

Equation (6) is the so-called adjoint problem, Eq. (7) is the optimization equation on the set of parameters $\mathbf{g}$, and Eq. (8) recovers the original state equations.

A. Drag force sensitivity based on an adjoint approach

For the work carried out in this study, the flow physics are governed by the following incompressible Navier–Stokes equations:

$$\frac{\partial \mathbf{u}}{\partial t} + \mathbf{u}\cdot\nabla\mathbf{u} - \nabla\cdot\sigma(p,\mathbf{u}) = \mathbf{f}, \tag{9}$$

$$\nabla\cdot\mathbf{u} = \mathbf{0} \quad \text{in } \Omega, \tag{10}$$

where Ω is the considered control volume around an immersed body. The imposed boundary conditions are $\mathbf{u} = \mathbf{g}$ on the boundary of the body, Γ, constant velocity $\mathbf{u} = \mathbf{u}_0$ at the inflow, and a pressure condition enforced as $p\mathbf{n} - \frac{1}{\mathrm{Re}}\nabla\mathbf{u} = 0$ at the outflow. Note that the velocity boundary condition at the body surface, Γ, is related to the parameter vector, $\mathbf{g}$. The interpretation of $\mathbf{g} = \mathbf{0}$ is a non-slip wall condition or a blowing/suction actuation mechanism. Re is the Reynolds number of the fluid flow, $\mathbf{f}$ considers the application of a forcing term, and σ is the stress tensor. The stress tensor is defined as

$$\sigma(p,\mathbf{u}) = -pI_d + \frac{1}{\mathrm{Re}}(\nabla\mathbf{u} + \nabla\mathbf{u}^T). \tag{11}$$

The state of the system, $\mathbf{q} = (\mathbf{u}, p)$, depends on the non-dimensionalized velocity and pressure vectors with respect to the characteristic body length and the free stream velocity. Finally, its L^2- inner product may be expressed as

$$\int_V \mathbf{q}\mathbf{q}'\mathrm{d}V = \int_V (\mathbf{u}\cdot\mathbf{u}' + pp')\mathrm{d}V. \tag{12}$$

Applying the aforementioned formulation to a fluid flow problem and considering the cost function as the mean drag force, $\bar{D} = \frac{2}{T}\int_0^T\int_\Gamma \sigma(\mathbf{u},p)\mathbf{n}\cdot\mathbf{e}_x \mathrm{d}\Gamma\mathrm{d}t$, where $\mathbf{n}$ is the normal vector around the surface of the body, the Lagrangian is redefined as

$$\mathscr{L} = \bar{D} - \frac{1}{T}\int_0^T\int_\Omega \mathbf{u}^\dagger\cdot\left(\frac{\partial\mathbf{u}}{\partial t} + \mathbf{u}\cdot\nabla\mathbf{u} - \nabla\cdot\sigma(p,\mathbf{u}) - \mathbf{f}\right)\mathrm{d}\Omega\mathrm{d}t - \frac{1}{T}\int_0^T\int_\Omega p^\dagger\nabla\cdot\mathbf{u}\mathrm{d}\Omega\mathrm{d}t, \tag{13}$$

where $\mathbf{e}_x$ is the projection direction of the drag force and $\lambda = (\mathbf{u}^\dagger, p^\dagger)$ are the adjoint variables associated with each equation.

The expression for the drag force sensitivity with respect to the introduction of external force perturbations may be formulated as

$$\nabla_\mathbf{f} D = \mathbf{u}^\dagger, \tag{14}$$

and to a perturbation on the boundary condition of the body surface, $\mathbf{g}$, as

$$\nabla_\mathbf{g} D = \sigma(-p^\dagger, \mathbf{u}^\dagger)\mathbf{n} + (\mathbf{g}\cdot\mathbf{n})\mathbf{u}^\dagger. \tag{15}$$

The reader may note that the second term of Eq. (15) depends on the velocity boundary condition imposed on the body surface, $\mathbf{g}$. In the case of non-slip conditions imposed at the surface, this term is canceled. However, if this formulation is applied to boundaries with blowing-suction actuation, it needs to be kept. The complete development for both steady and unsteady flow formulations is gathered in Appendix, Subsections 1 and 2.

B. Drag force sensitivity to surface morphing

A mathematical framework is presented below with the aim of obtaining an analytical formulation to provide the sensitivity of the drag force to modifications in the geometry of the body surface, from which we may additionally obtain an interpretation of the physics of the fluid problem.

Once the sensitivity to changes in the boundary condition has been calculated, it may be used to obtain the sensitivity to changes of geometry, using the following theorem:

Let Γ_0 is the initial boundary of the surface body, $(\mathbf{u}, p)$ is the solution of the Navier–Stokes equations, and Γ' is a perturbation on the boundary. The perturbation flow, $(\mathbf{u}', p')$, induced by the variation of the boundary satisfies the linearized Navier–Stokes equations with the following boundary condition on the cylinder:

$$\mathbf{u}' = -\frac{\partial\mathbf{u}}{\partial\mathbf{n}}(\mathbf{v}\cdot\mathbf{n}), \tag{16}$$

where $\mathbf{v}$ is defined by $\Gamma_0 - \Gamma'$. That is, at first order, we have an identification of a perturbation in the geometry with one in the boundary conditions. The reader is referred to Gunzburger[24] or Sokolowski and Zolésio[30] for more details on the aforementioned formulation.

If this theorem is applied with the aim of obtaining the drag sensitivity with respect to surface morphing, considering this particular boundary perturbation, then the following expression is obtained for the sensitivity of the cost function with respect to changes in the body geometry or shape sensitivity:

$$\nabla_\Gamma D = -\left(\sigma(-p^\dagger,\mathbf{u}^\dagger)\mathbf{n}\cdot\frac{\partial\mathbf{u}}{\partial\mathbf{n}}\right)\mathbf{n} - \left(\mathbf{u}^\dagger\cdot(\mathbf{g}\cdot\mathbf{n})\frac{\partial\mathbf{u}}{\partial\mathbf{n}}\right)\mathbf{n}. \tag{17}$$

We may refer to Eq. (17) as the sensitivity of the cost function to modifications in the body surface geometry or drag shape sensitivity. Imposing $\mathbf{u}^\dagger = 2\mathbf{e}_x$ on Γ, see Appendix, Subsection 3 for details, the aforementioned expression may be reformulated as

$$\nabla_\Gamma D = -\left(\sigma(-p^\dagger,\mathbf{u}^\dagger)\mathbf{n}\cdot\frac{\partial\mathbf{u}}{\partial\mathbf{n}}\right)\mathbf{n} - \left(2\mathbf{e}_x\cdot(\mathbf{g}\cdot\mathbf{n})\frac{\partial\mathbf{u}}{\partial\mathbf{n}}\right)\mathbf{n}. \tag{18}$$

One may note that the sensitivity to changes in geometry is the projection of the sensitivity to perturbations at the boundary condition on the cylinder onto the normal derivative of the velocity on the surface. This facilitates its calculation, while $\nabla_\mathbf{g} D$ has been previously calculated,

$$\nabla_\Gamma D = \left(\nabla_\mathbf{g} D, -\frac{\partial\mathbf{u}}{\partial\mathbf{n}}\mathbf{n}\right)\mathbf{n}. \tag{19}$$

C. Physical interpretation of the sensitivity function

The advantage of using this formulation is that it allows us to reveal the physical meaning of the interaction between the adjoint flow and the shear flow. Let us now look at each of the two terms of Eq. (18),

1. $-(\sigma(-p^\dagger,\mathbf{u}^\dagger)\mathbf{n}\cdot\frac{\partial\mathbf{u}}{\partial\mathbf{n}})\mathbf{n}$.

   This term is directly a correction in the normal direction of the force exerted by the flow on the body. To see this, we take a perturbation such as $\mathbf{v} = \alpha\mathbf{n}\delta(\mathbf{x} - \mathbf{x}_0)$, where $\delta(\mathbf{x})$ is the Dirac delta

distribution, $\alpha \ll 1$, and $\mathbf{x}_0$ is a point on the surface of the body. The new drag coefficient becomes

$$D' \sim \int_\Gamma 2\sigma(\mathbf{u},p)\mathbf{n}\cdot\mathbf{e}_x - \alpha\left(\sigma(-p^\dagger,\mathbf{u}^\dagger)\mathbf{n}\cdot\frac{\partial\mathbf{u}}{\partial\mathbf{n}}\right)\delta(\mathbf{x}-\mathbf{x}_0)\mathrm{d}\Gamma, \quad (20)$$

where it is obtained by perturbing the stress tensor at $\mathbf{x}_0$

2. $-(2\mathbf{e}_x\cdot(\mathbf{g}\cdot\mathbf{n})\frac{\partial\mathbf{u}}{\partial\mathbf{n}})\mathbf{n}$.

In this case, we have the balance between the boundary condition and the normal direction of the body, but more interesting is the balance between the adjoint velocity and the normal projection of the boundary condition. As the drag-adjoint velocity is $2\mathbf{e}_x$ around the cylinder, regardless of the original boundary condition, this term becomes negligible close to the areas where the normal vector to the surface is perpendicular to $\mathbf{e}_x$.

III. NUMERICAL METHODS

In Secs. III–V, we consider a two-dimensional circular cylinder immersed in an incompressible laminar flow. The rectangular computational domain is defined by $\Omega\{(x,y)|\, x\in[-40d,50d],\ y\in[-40d,40d]\}/\Gamma$, where d is the diameter of the cylinder and Γ denotes its surface, defined by $\Gamma=\{(x,y)|x^2+y^2<d^2\}$. The flow physics is defined by the Reynolds number, $\mathrm{Re}=u_\infty d/\nu$, based on the cylinder diameter. The fluid density, ρ, and the kinematic viscosity, ν, are assumed constant. The Reynolds regime is then adjusted by the free-stream velocity, u_∞. In this work, we have considered $\mathrm{Re}=20$ and $\mathrm{Re}=100$ for the validation cases, and $\mathrm{Re}=40$ and $\mathrm{Re}=100$ for the analysis of the shape sensitivity, steady and unsteady cases for each section, respectively.

The governing equations are implemented in FEniCS,[31] an open source solver for partial differential equations based on finite elements. The unsteady Navier–Stokes equations are solved with Chorin's algorithm.[32] Regarding the boundary conditions, a constant velocity was set at the upstream limit of the computational domain, while a static pressure condition was imposed at the downstream outlet. Slip walls were considered for the upper and lower limits, i.e., $\mathbf{u}=(1,0)=\mathbf{u}_0$, and a non-slip condition was set at the cylinder surface. This was imposed by enforcing $\mathbf{g}=0$ for the calculation of the flow solution, as described in Sec. II.

The mesh is generated with FEniCS, considering two refinement areas: one on $\{(x,y)|\, x\in[-9d,24d],\ y\in[-9d,9d]\}$ and the second located in the vicinity of the cylinder surface on $\{(x,y)|\, x\in[-3d,12d],\ y\in[-3d,3d]\}$ (see Fig. 1). Mesh independence is first evaluated in steady flow ($\mathrm{Re}=40$), monitoring the drag forces and the flow separation point given by the angle θ. Then, for unsteady flow ($\mathrm{Re}=100$) throughout the evaluation of the associated wake flow Strouhal number, $\mathrm{St}=fd/u_\infty$, where f is the frequency of vortex shedding and the value of the mean drag coefficient, $C_D=D/0.5\rho u_\infty d$. In the unsteady simulation, the wake remains laminar, with a periodic shedding of vortexes that form the so-called Von-Kármán vortex street. To properly capture this phenomenon, we considered a time step of $\Delta t=1/(10\mathrm{St})$ seconds. The temporal convergence of the simulations was ensured by evaluating wake flow time series following the criteria of Clark and Grover.[33] After the wake develops and the force time series reaches temporal convergence (this normally occurs after 20 oscillation periods), the flow solution is computed for 60 more periods. For the calculation of the unsteady adjoint, we need to store each time step of the flow solution to solve the adjoint equations backward in time using the same time step.

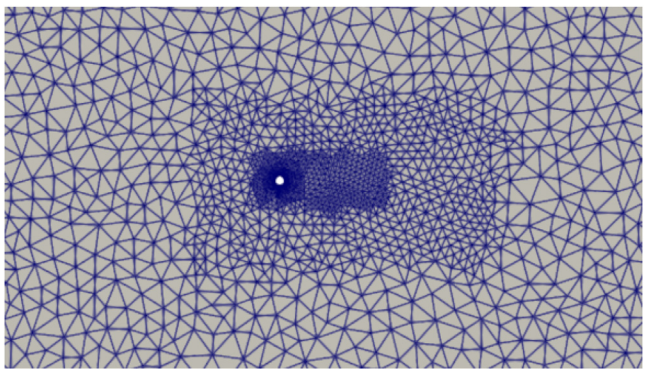

FIG. 1. Computational mesh with 11 700 elements where different refinement areas are shown.

Table I encompasses the data collected for the drag coefficient and the separation point ($\mathrm{Re}=40$) as well as the average drag coefficient and Strouhal number for the unsteady case ($\mathrm{Re}=100$). The relative error of each observable is calculated between two consecutive meshes. Note how the evolution of the physical observables as a function of the number of elements of the mesh reaches a good convergence. For the following simulations, the mesh with 11 700 elements is used (see Fig. 1), where 1280 of these elements are located on the cylinder surface.

A. Flow solution validation

To ensure the precision of the numerical methodology presented, several fundamental flow properties of the calculated two-dimensional flow around a circular cylinder are compared with the reference data for steady[34,35] and unsteady[29] flows. For comparison, the relative error between the reference and numerical values is computed, $\varepsilon=\frac{|v_{\mathrm{ref}}-v_{\mathrm{num}}|}{v_{\mathrm{ref}}}(\%)$.

Steady flow solutions were obtained at $\mathrm{Re}=40$, monitoring the drag coefficient and the flow separation point measured on the surface of the cylinder. Table II shows a good agreement between the reference and numerical data.

A developed unsteady regime was recovered for $\mathrm{Re}=100$, extracting the time-averaged drag coefficient and the Strouhal number. For the calculation of the Strouhal number, the frequency, f, was calculated from the time series of the vertical component of the velocity at the point $(x,y)=(6d,0)$. Table III shows the comparison between the reference and numerical data.

B. Adjoint flow validation. Sensitivity of the drag force to a perturbation of external forcing

The drag force sensitivity is first obtained by applying Eq. (14) to a steady flow solution at $\mathrm{Re}=20$. Figure 2 depicts the sensitivity field associated with a perturbation of external forcing, $\mathbf{f}'$. The magnitude of the adjoint field is related to the zones where the drag force is more sensitive to perturbations in the external force. These results are consistent with those obtained by Wang and Gao,[36] who suggested that

TABLE I. Convergence of physical observables. Drag coefficient and bubble separation are calculated at Re = 40. Strouhal number and mean drag coefficient are calculated at Re = 100. The values within parentheses represent the relative errors of the observables between two consecutive meshes.

Number of elements	Drag coefficient, C_D		Bubble separation, θ (°)		Strouhal number, St		Mean drag coefficient, $C_{\bar{D}}$	
7622	1.5070	···	51.48	···	0.1637	···	1.5932	···
8640	1.5123	(−0.35%)	52.61	(−2.20%)	0.1639	(−0.12%)	1.5602	(2.07%)
9630	1.5148	(−0.17%)	53.46	(−1.62%)	0.1642	(−0.18%)	1.3757	(11.83%)
11 700	1.5167	(−0.13%)	53.52	(−0.11%)	0.1643	(−0.06%)	1.3462	(2.14%)
13 280	1.5170	(−0.02%)	53.51	(0.02%)	0.1643	(0.00%)	1.3459	(0.02%)

TABLE II. Drag coefficient and flow separation point on the cylinder surface, comparing between numerical and reference values for steady flow, Re = 40.

	Reference	Present	ϵ
Drag coefficient, C_D (Ref. 34)	1.5187	1.5167	0.13%
Bubble separation, θ (Ref. 35)	53.50°	53.52°	0.04%

TABLE III. Strouhal number and mean drag coefficient comparison between numerical and reference values for unsteady flow, Re = 100.

	Reference 29	Present	ϵ
Strouhal number, St	0.166	0.164	1.2%
Mean drag coefficient, $C_{\bar{D}}$	1.3363	1.3462	0.4%

the adjoint velocity is an upstream jet generated by the boundary condition around the cylinder, acting as downstream suction.

If the flow configuration of interest lands in an unsteady regime, the unsteady version of Eq. (14) must be applied. Figure 3 illustrates the evolution of the unsteady adjoint field, colored by the magnitude of the adjoint velocity, for a flow solution obtained at Re = 100. In the figure, three snapshots cover half of a shedding period ($T/6$, $T/3$, and $T/2$), depicting how throughout the temporal evolution the most sensitive regions swap from upper to lower regions of the cylinder every half period of the vortex's shedding. Again, the results shown here are in agreement with the reference data Wang and Gao.[36]

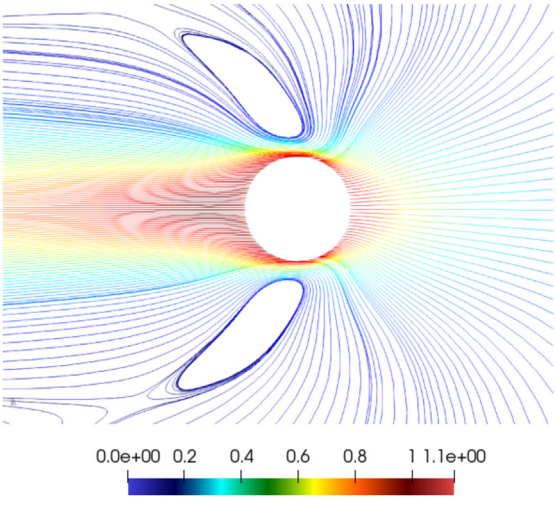

FIG. 2. Sensitivity of the drag force due to a perturbation caused by external forcing at Re = 20.

C. Sensitivity of the drag force to body surface boundary conditions perturbations

In this section, the sensitivity of the drag force to a perturbation of the body boundary condition in the unsteady regime is obtained and compared with the results of Meliga *et al.*,[29] who studied the flow over a circular cylinder at Re = 100. Considering a non-slip wall condition imposed at the cylinder surface, the drag sensitivity due to perturbations in the boundary condition, Eq. (15), simplifies to

$$\nabla_{\mathbf{g}}\bar{D} = \sigma(-p^{\dagger}, \mathbf{u}^{\dagger})\mathbf{n}. \tag{21}$$

Figure 4 gathers the evolution of the calculated sensitivity throughout a period of vortex shedding, expressed as a vector field distributed on the surface of the body, which is in good alignment with the prediction of the reference data.[29] This field indicates the direction of the velocity boundary condition to be applied on the surface of the body to minimize drag. If the field points inward, it is interpreted as a suction mechanism, and as a blowing mechanism if it points outward.

Figure 4(a) depicts a suction distribution on the upper half of the cylinder's surface, together with a blowing of lesser magnitude over the lower half. Figure 4(b) depicts that the transition from one pattern to the other is accompanied by a distortion of the blowing velocity at the rear surface, is found to be stronger on the half of the cylinder at which suction is applied, and is accompanied by an almost constant blowing on the front surface. Figures 4(c) and 4(d) show the same pattern of substantial suction and lesser blowing and transition, just that both halves of the cylinder surface exchange roles because the phase is shifted by half a shedding period.

IV. RESULTS

In this section, the sensitivity of the drag force to surface morphing is calculated for a two-dimensional circular cylinder using Eq. (18). The numerical methodology is first applied to steady flow solutions, and the evolution of the drag coefficient is compared with that predicted by the theoretical framework presented here. Afterward, the unsteady adjoint flow solution is obtained, and a time-dependent sensitivity vector field is recovered. Both a time-dependent surface morphing and a single surface deformation based on the

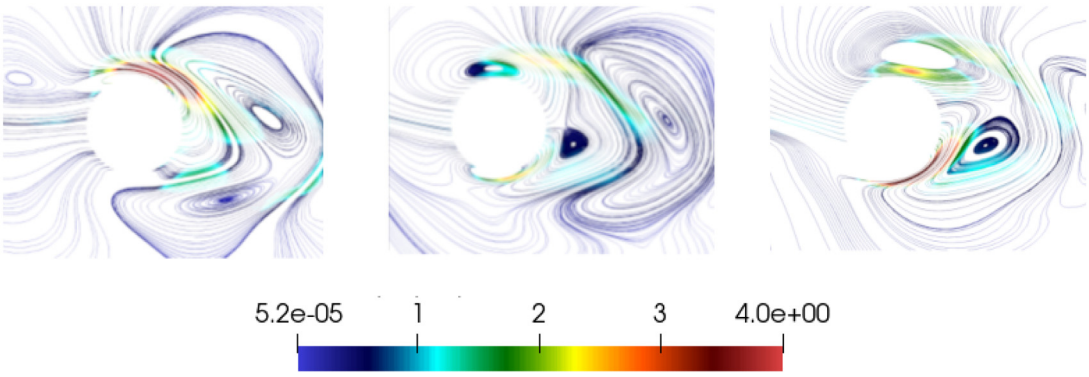

FIG. 3. Temporal evolution of the drag sensitivity due to a perturbation of external forcing. The snapshots of cover half of a vortex shedding period, $T/2$, at Re = 100. The time evolution has to be interpreted from left to right, where there is a temporal step of $T/6$.

time-averaging of the sensitivity field are computed and compared against one another.

A. Drag sensitivity for steady flow conditions: Re = 40

The application of Eq. (18), considering a boundary condition of $\mathbf{g} = 0$, provides a vector field around the cylinder describing the drag sensitivity with respect to surface morphing, as shown in Fig. 5(a). Each node has an associated vector that indicates the direction in which to move each point, note that it does not have to be normal to the surface or a relative magnitude. The most sensitive areas are symmetrically located at the upper and lower zones of the cylinder's surface, corresponding to areas with lower local pressure and higher local velocity, together with less sensitive regions near the stagnation point. The aft part of the body surface, where the flow is already separated, presents as having neglecting sensitivity to local deformations.

A surface morphing conducted by the sensitivity field toward a drag force reduction presents a reduction of the cylinder radius at the lower and upper regions, contracting the body, and a smaller outward deformation in the vicinity of the stagnation point, flattening the surface. The new surface shape is defined as $\Gamma' = \Gamma - \alpha \nabla_\Gamma D$, where α is a scalar used as a control parameter.

In Fig. 6, the behavior of the pressure coefficient and the sensitivity around the cylinder are presented, highlighting the area where the flow is separated. Areas of high sensitivity are those of lower pressure, whereas surface sensitivity is marginal in separated flow regions. Figure 7 depicts the quantitative drag reduction with respect to deformation. Both finite difference results and the first order derivative are compared, showing that in both cases, a linear evolution of the drag is kept up to values of $\alpha = 0.01$. This is in line with the mathematical formulation presented in Sec. II B, recalling how, in a first-order approximation, a perturbation of the surface geometry is equivalent to a specific velocity distribution on the surface boundary condition, which may be expressed as

$$\mathbf{g}' = -\frac{\partial \mathbf{u}}{\partial \mathbf{n}}(\alpha \nabla_\Gamma D \cdot \mathbf{n}), \tag{22}$$

where α is the magnitude of the deformation.

The new estimated value for the drag force after the surface morphing may then be calculated as follows:

$$D = D_0 - \langle \nabla_{\mathbf{g}} D, \mathbf{g}' \rangle_\Gamma = D_0 - \alpha \left\langle \nabla_{\mathbf{g}} D, -\frac{\partial \mathbf{u}}{\partial \mathbf{n}}(\nabla_\Gamma D \cdot \mathbf{n}) \right\rangle_\Gamma, \tag{23}$$

where D_0 is the initial drag force value and $\langle \nabla_{\mathbf{g}} D, \mathbf{g}' \rangle_\Gamma = \int_\Gamma \nabla_{\mathbf{g}} D \cdot \mathbf{g}' d\Gamma$ is the estimated drag force reduction. Taking into account a deformation parameter of $\alpha = 0.005$, the relative error is $\varepsilon = \frac{|v_{\text{theoretical}} - v_{\text{numerical}}|}{v_{\text{theoretical}}} = 3.3\%$.

B. Drag sensitivity for unsteady flow conditions: Re = 100

In this section, we now apply Eq. (18) to a unsteady flow solution. In this case, the recovered sensitivity field is time-dependent, and hence, a different treatment is required for the reduction of the drag force. Two approximations are applied. First, the time-integration of the sensitivity field is taken, to obtain a single deformation based on the unsteady adjoint calculation over a time period, T,

$$\overline{\nabla_\Gamma D} = \frac{1}{T}\int_0^T \nabla_\Gamma D dt. \tag{24}$$

Afterward, we evaluate the drag behavior by deforming the cylinder's surface at each time step according to the time-dependent sensitivity.

1. Mean deformation

Taking into account for a single surface deformation based on the averaging of the calculated gradients, the new shape of the body is defined by $\Gamma' = \Gamma - \alpha \overline{\nabla_\Gamma D}$, where the applied vector field is shown in Fig. 5(b). In the test case analyzed here, a value of $\alpha = 0.01$ reports a change of radius 16% in the areas with maximum sensitivity.

Similar to the results obtained in the steady case, the vector field possesses a very sensitive area at the poles of the body following an almost normal direction, indicating that a drag reduction would be achieved, contracting the body in these areas, together with an outward deformation flattening the frontal section of the body. On the contrary, the vector field of the front and aft parts of the body presents a similar magnitude of sensitivity.

As expected, as the deformation increases, the average drag is reduced. Additionally, an increase in deformation is also accompanied

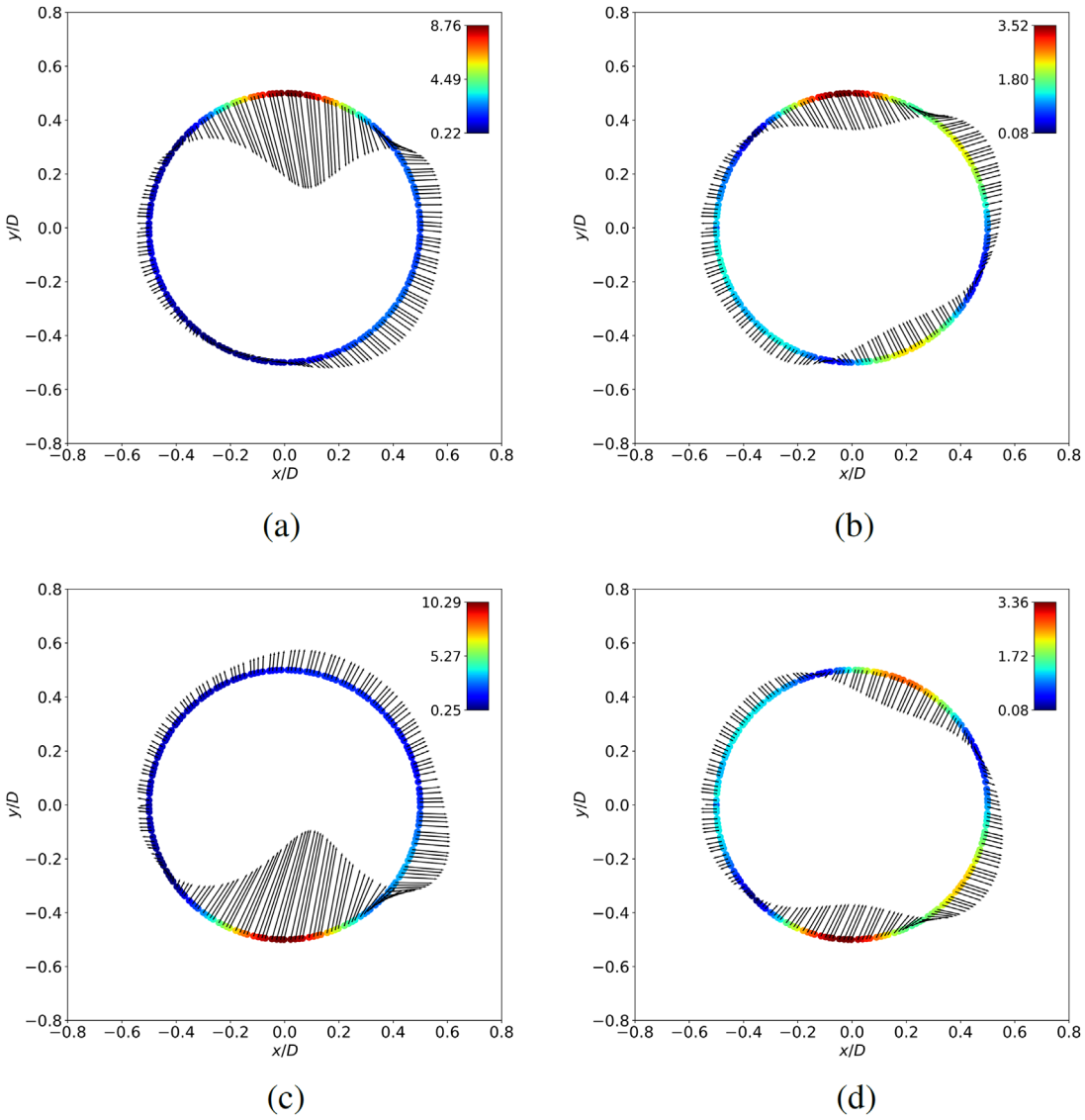

FIG. 4. Temporal evolution of the vector field corresponding to the drag force sensitivity to body boundary condition modifications over a shedding period, T, at Re = 100. Images are separated by a temporal step of $T/4$. (a) The maximum rise in the cylinder part and (b) the transition of the boundary condition to a suction mechanism of the lower part. (c) and (d) The symmetrical to the behavior in the lower part of the cylinder.

by a reduction in the oscillation amplitude of the drag coefficient. Figure 8 depicts the behavior of the drag coefficient for progressive surface deformations throughout the temporal window analyzed. Within the figure, the deformed shape of the body surface is also presented. In Table IV, the results are numerically presented as a function of the morphing control parameter, α, reflecting how as the mean drag decreases, the amplitude of the oscillation is reduced. Flattening of the upper and lower regions of the cylinder also affects the frequency of the vortex shedding, modifying the associated frequency. Due to the modifications in the position and angle of the shear layers caused by the surface deformations, favoring their interaction as the body is contracted, further deformations imply an increase in the vortex shedding frequency.

These results were also observed by Martinez-Cava *et al.*[37] and Brewster and Juniper[38] on the analysis and control of the first instability of the cylinder wake by means of surface deformation. In both papers, the sensitivity of the unstable mode at Re = 40–50 is studied. In both papers, the sensitivity of the unstable mode at Re = 40–50 is studied. In particular, significant similarities have been observed between the results obtained from both approaches. These similarities suggest a potential correlation between the strategies employed to reduce drag force and the modifications in the geometry of unstable flow modes, since the drag force decreases with the amplitude of oscillation in these regimes. This finding supports the notion that adjoint methods can provide valuable insights into the necessary geometry

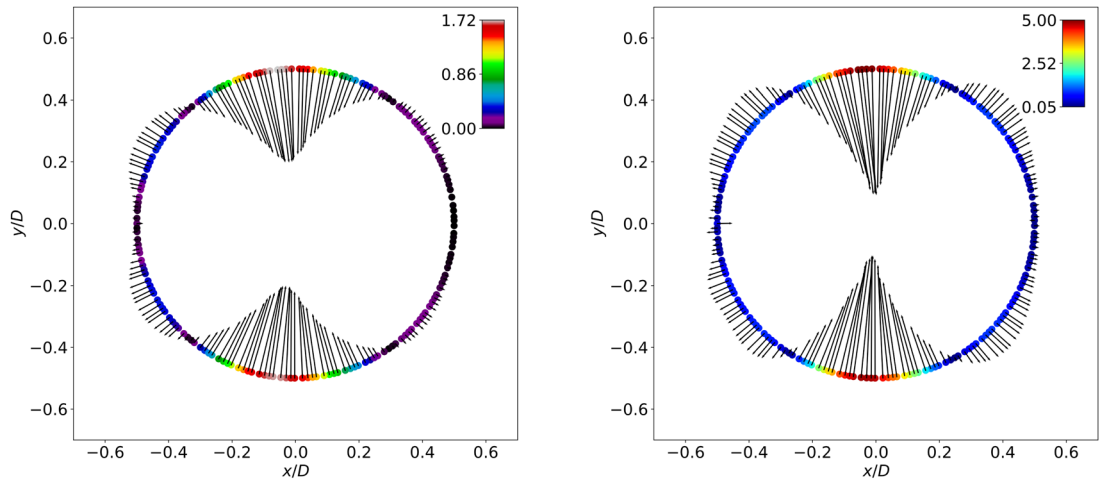

FIG. 5. (a) Vector field of the shape sensitivity of the drag force in steady flow: Re = 40. (b) Vector field of the shape mean sensitivity of the mean drag force in unsteady flow: Re = 100.

modifications to optimize flow behavior with respect to drag force. Therefore, it is concluded that there exists an inherent connection between the two methods and their ability to enhance aerodynamic efficiency around the body of interest.

In the same manner as in the steady case, Fig. 9 depicts the variation of the sensitivity magnitude and the averaged pressure coefficient around the cylinder, indicating the area of the separated flow. The sensitivity to local deformation changes sign at these regions, characterized by the strong adverse pressure gradient due to the cylinder's curvature. As expected, a drag reduction may be achieved by a local increase on the cylinder's radius at these locations, reducing the curvature and, thus, smoothing the pressure gradients. The crests of the cylinder, where the lowest values of static pressure are present before the change in sign of the pressure gradient, are revealed again to be more sensitive to surface perturbations.

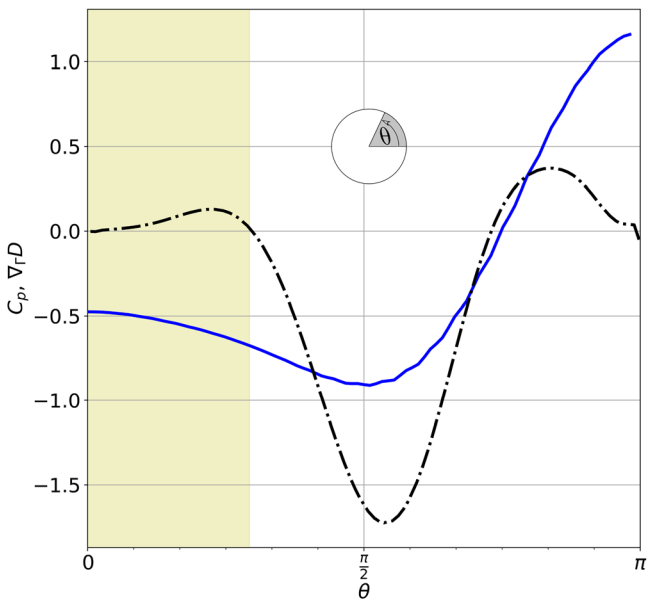

FIG. 6. Comparison of the pressure coefficient and sensitivity behavior at Re = 40. The blue line represents C_p, and the dotted line represents $\nabla_\Gamma D$. The shaded area is the area where the flow is detached.

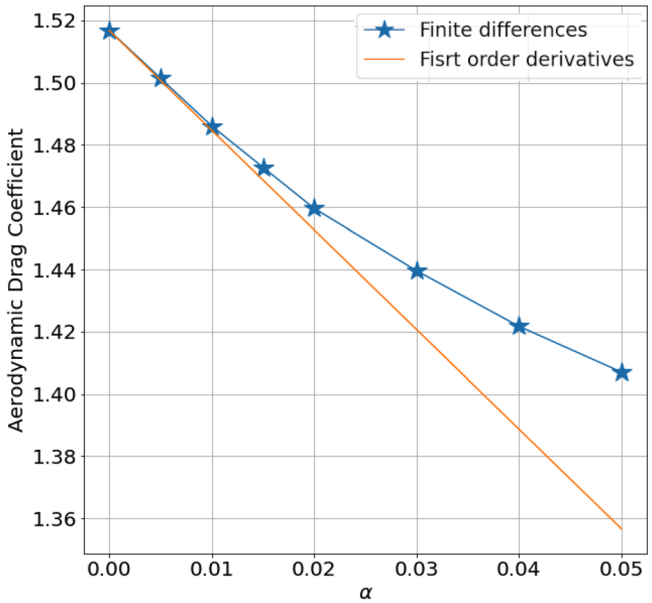

FIG. 7. Drag force coefficient as a function of the surface deformation control parameter, α. Numerical results are obtained for steady flow conditions, at Re = 40.

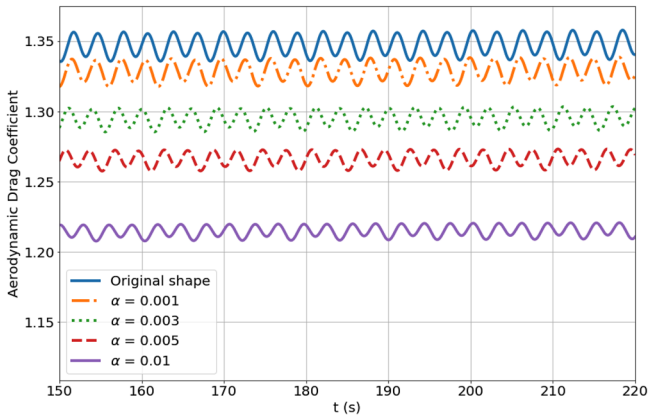

FIG. 8. Drag coefficient time series for different values of the morphing parameter, α.

TABLE IV. Quantitative increments caused by the surface deformation. Mean drag, ΔD, and oscillation amplitude, $\Delta\sigma_D$, of the calculated drag time series as a function of the morphing parameter, α.

α	ΔD	$\Delta\sigma_D$
0.001	0.018	0.020
0.002	0.035	0.019
0.003	0.052	0.017
0.005	0.081	0.015
0.01	0.131	0.012

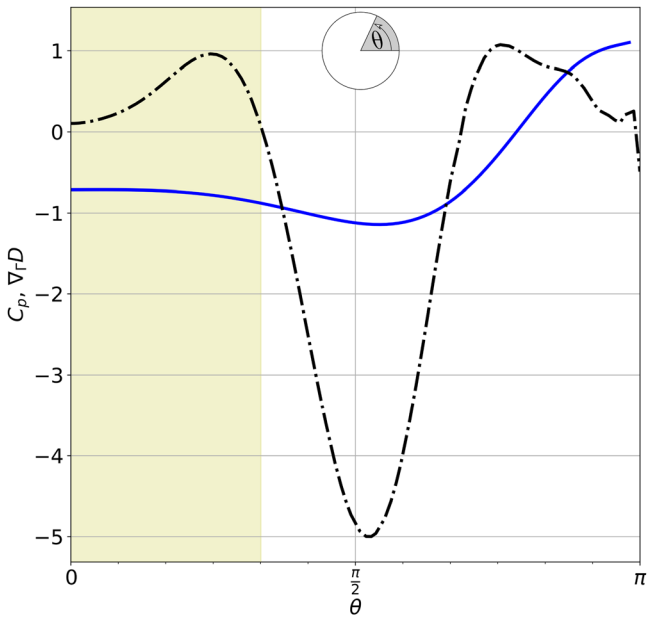

FIG. 9. Pressure coefficient, C_p, the solid line, and drag sensitivity, $\nabla_\Gamma D$, the dotted line over the cylinder surface at Re = 100. Areas of separated flow are shaded.

Despite the well-known physics of the flow around a two-dimensional cylinder, in which context, the aforementioned analysis may not add novel information regarding the physics related to flow separation and pressure drag forming, one may take into account that the surface sensitivity has been obtained from a mathematical development of the Navier–Stokes adjoint equations, with no contextualization on the problem of ubiquitous flow physics. The analysis of this flow configuration serves to correlate the obtained results for the drag force sensitivity to local deformations with the well studied drag sources of the flow around a cylinder.

2. Instantaneous deformation

In this analysis, we evaluate the drag force behavior using a local surface morphing performed at each time step, following the calculated time-dependent sensitivity field. Figure 10 gathers four equispaced snapshots of the temporal evolution of the drag force sensitivity throughout a vortex shedding time period and the vorticity production on the wake at that instant. The sensitivity vector field presents a symmetrical behavior with respect to the middle plane, in an alternate manner related to the shedding of the vortices. Figures 10(a) and 10(b) depict the vector field when the upper and lower vortices are forming, respectively, right after the separation of the previous vortex on the alternate side. Figures 10(c) and 10(d) correspond to the sensitivity vector field present just before the separation of the vortices. The direction and magnitude of the drag sensitivity field is directly related to the periodic pressure gradients along the cylinder's surface. A description of the sensitivity regions and the predicted changes in flow physics due to surface morphing guided by the drag sensitivity field are described here.

On the vortex-formation side, the magnitude of the sensitivity field increases with the vorticity production, while reducing on the opposite side until it becomes negligible. A time-dependent surface morphing would alter the surface by means of reducing the surface curvature on the vortex-formation side and therefore reducing the base region area. This facilitates the interaction between the shear layers and accelerates the shedding frequency. When the vortex separates, the magnitude and direction of the vector field shifts toward the opposite side of the cylinder. At first, a highly sensitive region develops near the flow separation point, suggesting a reduction of the curvature by increasing the cylinder's radius in this area, facilitating boundary layer attachment. As the vortex grows in the base region, the sensitivity field adopts the above-mentioned distribution on the vortex-formation side while reducing its magnitude on the opposite side.

Following a surface modification guided by the sensitivity field leads toward the reduction on the vorticity production at the base region, with smoother surface pressure gradients, eventually reducing the pressure drag contribution through these local deformations.

The time-dependent shape is, therefore, defined by the expression $\Gamma(t) = \Gamma - \alpha\nabla_\Gamma D(t)$, with α as a deformation control parameter. Figure 11 depicts the temporal evolution of the drag coefficient for several values of α, which can be compared with the mean drag coefficient values obtained for several deformations gathered in Figs. 12(a) and 12(b). The predicted linear behavior is quickly lost for relative small deformations, making a quantitative prediction difficult.

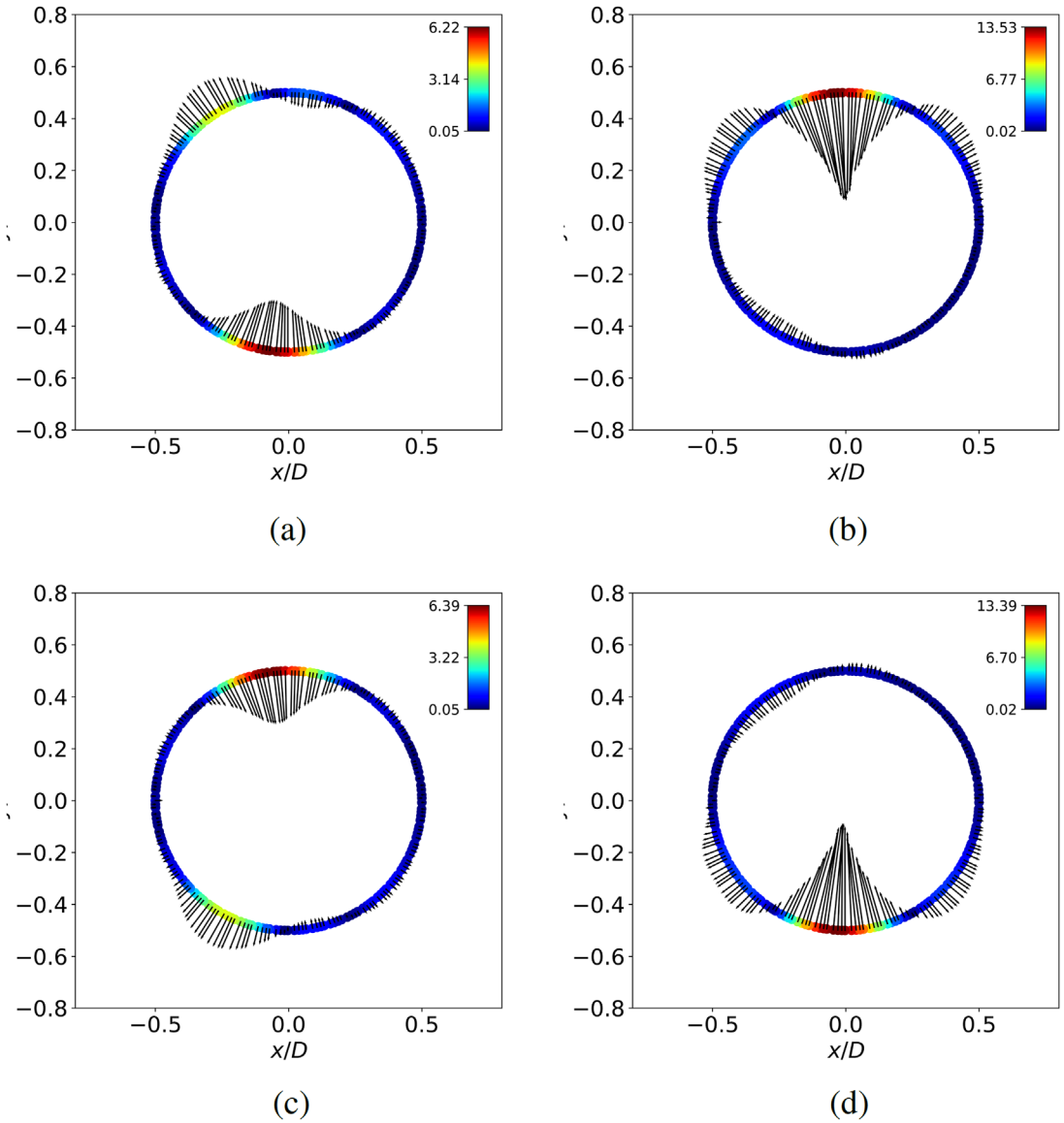

FIG. 10. Temporal evolution of the sensitivity vector field throughout a flow oscillation period, calculated at Re = 100. Images are separated by a temporal step of $T/4$. (a) A small contraction in the lower part and expansion in the upper part and (b) the maximum contraction in the upper part. (c) and (d) The symmetrical to the behavior in the lower part. Vorticity maps at each subfigure complement the plots with the physical formation of the wake vortices.

3. Instantaneous vs mean deformation

The results collected in Sec. IV B suggest that a single deformation based on the time integration of the sensitivity field is more efficient in reducing body drag than in deforming the surface at each time step following the distribution of the sensitivity vector field. This phenomenon is counter intuitive since, due to the unsteady nature of the vortex shedding, it may appear that a time-dependent deformation would result in better performance for the body morphing.

The underlying physics is explained here with a mathematical subtlety present in the developed theoretical framework. For the calculation of the adjoint field, it is necessary to calculate the entire flow history. Once the adjoint equations have been solved backward in time, Eq. (18) is used to calculate the sensitivity field using the flow and adjoint solutions. The evaluation of the sensitivity performance is then based on the application, at each time step, of a deformation that follows the recovered sensitivity vector field. This modified geometry induces a flow behavior different from the original geometry, but in the next time step, the surface will be deformed according to the function calculated from the original flow solution. Therefore, a mismatch occurs between the vector field obtained for the original body geometry and the one that would be recovered for the flow solution produced with the deformed body. To reinforce this argument, deformations at

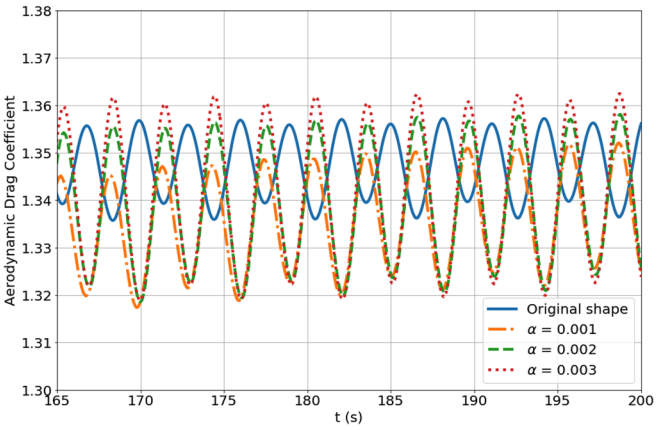

FIG. 11. Evolution of drag coefficient by several instantaneous deformations.

low α values, as shown in Fig. 12(b), have been performed, and linear behavior is not observed. However, if a time-averaged vector field is used, the observable physical property being optimized is the mean drag, and this problem does not arise.

V. CONCLUSIONS

An adjoint approach is developed to analyze the sensitivity of the drag force to surface morphing of a body immersed in an incompressible flow. Through a bijection between a perturbation of the geometry and the body surface boundary condition at first order, an analytical expression of the drag sensitivity to changes in the geometry of the body and its relation to the sensitivity to boundary condition perturbations are derived from the Navier–Stokes adjoint equations. From a continuous approach, the proposed novel methodology is presented as a powerful tool to be applied in stationary and non-stationary flow configurations. Considering either the body surface boundary condition or the surface geometry, a vector field for the drag sensitivity is recovered.

The mathematical framework is first applied to a two-dimensional cylinder immersed in an incompressible steady flow, at $\mathrm{Re} = 40$. A substantial reduction of the drag coefficient is obtained when the body surface is deformed according to the calculated sensitivity field. Additionally, this reduction can be quantitatively predicted when the deformations are kept within a small range, thanks to the analytical expressions.

Extending the analysis to non-stationary flows, the same geometry is studied at $\mathrm{Re} = 100$. The sensitivity vector field is calculated from a temporal application of the adjoint equations, recovering a time-dependent function of the drag sensitivity. A comparison was made between a steady and an unsteady deformation, either time-averaging the calculated vector field or discretely applying it, deforming the body surface at each time step. A single deformation induced by the time-averaging of the sensitivity expression is shown to be extremely effective on the body drag force reduction. However, a time-dependent deformation did not achieve the same satisfactory results. A discussion of these results is presented, based on the mathematical development of the unsteady adjoint method. The physical implications of the drag sensitivity are extended in the discussion of the results, relating the magnitude and sign of the sensitivity vector field to the local flow variables. In the current case, where pressure drag sources dominate, the sensitivity to surface deformation is correlated with the evolution of the surface pressure coefficient, linking the mathematical development and flow physics.

The mathematical framework presented is applicable to anybody geometry without explicit parameterization, immersed in incompressible flows. Its potential for the analysis of unsteady flows widens and

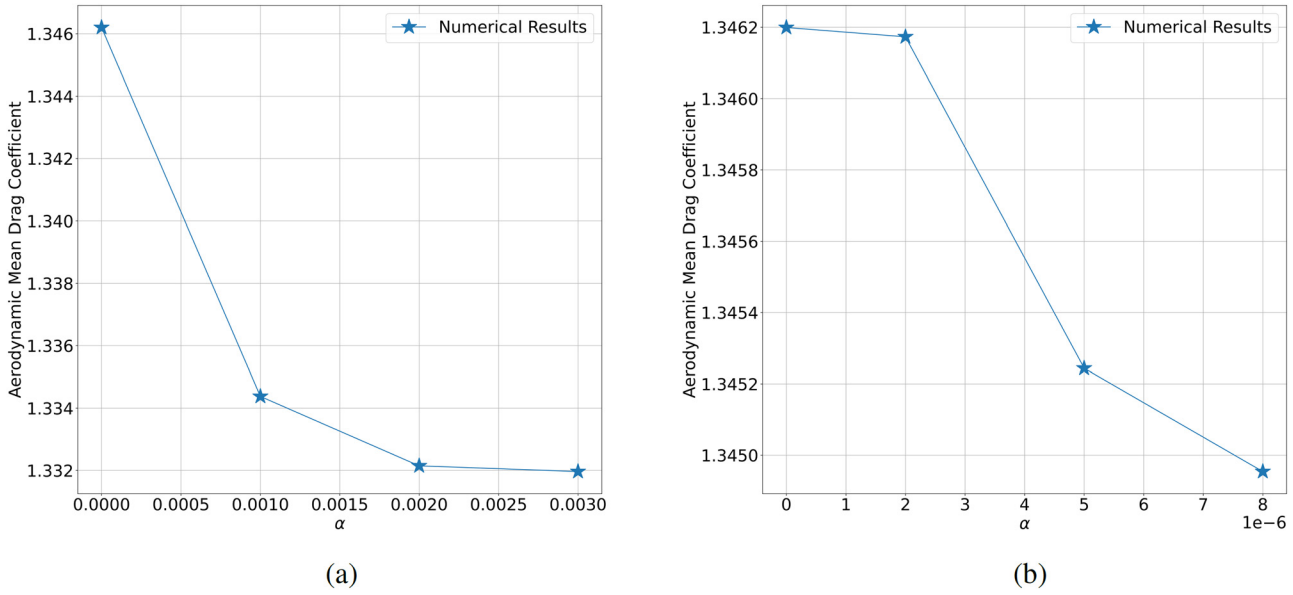

FIG. 12. Evolution of mean drag coefficient by several instantaneous deformations. (a) Mean drag force as a function of the surface deformation control parameter $\alpha \sim 10^{-3}$. (b) Mean drag force as a function of the surface deformation control parameter $\alpha \sim 10^{-6}$.

facilitates the application of surface morphing with drag force reduction purposes, such as the construction of an airfoil that can be adapted to each flow behavior.

ACKNOWLEDGMENTS

This research was supported by the Ministry of Education of Spain (No. PRE2019–087518) and by the European Union's Horizon 2020 research and innovation program under the Marie-Curie Programme GA-101019137, FLOWCID, and GA-955923, SSECOID.

AUTHOR DECLARATIONS

Conflict of Interest

The authors have no conflicts to disclose.

Author Contributions

Carlos J. Ruiz-Sanchez: Data curation (equal); Formal analysis (equal); Investigation (equal); Methodology (equal); Software (equal); Validation (equal); Writing – original draft (equal). **Alejandro Martínez-Cava:** Methodology (equal); Supervision (equal); Writing – review & editing (equal). **Miguel Chavez-Modena:** Methodology (equal); Supervision (equal); Writing – review & editing (equal). **Eusebio Valero:** Methodology (equal); Supervision (equal).

DATA AVAILABILITY

The data that support the findings of this study are available from the corresponding author upon reasonable request.

APPENDIX: CALCULATIONS FOR ADJOINT EQUATIONS AND SENSITIVITIES

1. Sensitivity of aerodynamic drag for a steady flow

The quantity of interest is the steady aerodynamic drag force around a body,

$$D = 2\int_\Gamma \{\sigma(p,\mathbf{u})\mathbf{n}\cdot\mathbf{e}_x\}d\Gamma, \tag{A1}$$

where $(\mathbf{u}, p)$ is the solution in the domain, Ω, of steady incompressible Navier–Stokes equations

$$\mathbf{u}\cdot\nabla\mathbf{u} - \nabla\cdot\sigma(p,\mathbf{u}) = \mathbf{f}, \tag{A2}$$

$$\nabla\cdot\mathbf{u} = \mathbf{0}, \tag{A3}$$

with the following boundary conditions: $\mathbf{u} = \mathbf{g}$ on the body boundary, Γ, $\mathbf{u} = (1,0)$ on the upper and lower walls of the domain, $\mathbf{u} = (1,0)$ at the inflow, and $pn - \frac{1}{Re}\nabla\mathbf{u} = \mathbf{0}$ at the outflow.

For the derivation of the sensitivity, we use the Lagrangian

$$\mathscr{L} = D - \int_\Omega \mathbf{u}^\dagger\cdot(\mathbf{u}\cdot\nabla\mathbf{u} - \nabla\cdot\sigma(p,\mathbf{u}) - \mathbf{f})d\Omega - \int_\Omega p^\dagger\nabla\cdot\mathbf{u}d\Omega, \tag{A4}$$

where $\mathbf{q}^\dagger = (\mathbf{u}^\dagger, p^\dagger)$ are the adjoint variables associated with the momentum equation and the conservation equation, respectively.

a. Adjoint equation for aerodynamics drag and sensitivities by an external force and by a perturbation of the body boundary condition

Introducing a perturbation on the force, $\mathbf{f} \to \mathbf{f} + \delta\mathbf{f}$, and a perturbation on the boundary condition, $\mathbf{g} \to \mathbf{g} + \delta\mathbf{g}$, the variation of the Lagrangian is defined as

$$\delta\mathscr{L} = \mathscr{L}(\mathbf{q}+\delta\mathbf{q}, \mathbf{q}^\dagger, \mathbf{f}+\delta\mathbf{f}) - \mathscr{L}(\mathbf{q}, \mathbf{q}^\dagger, \mathbf{f}). \tag{A5}$$

Using Eq. (A4) and Eq. (A1) into Eq. (A5) and developing it up to first order, we obtain the following expression:

$$\begin{aligned}\delta\mathscr{L} = {} & 2\int_\Gamma \{\sigma(\delta p,\delta\mathbf{u})\mathbf{n}\cdot\mathbf{e}_x\}d\Gamma \\ & - \int_\Omega \mathbf{u}^\dagger\cdot(\delta\mathbf{u}\nabla\mathbf{u} + \mathbf{u}\nabla\delta\mathbf{u} - \nabla\cdot\sigma(\delta p,\delta\mathbf{u}) - \delta\mathbf{f})\mathrm{d}\Omega \\ & - \int_\Omega p^\dagger\nabla\cdot\delta\mathbf{u}\mathrm{d}\Omega.\end{aligned} \tag{A6}$$

Then, integrating by parts the previous equation and using the Green's first identity, we get

$$\begin{aligned}\delta\mathscr{L} = {} & \int_\Gamma (\sigma(\delta p,\delta\mathbf{u})\mathbf{n}(2\mathbf{e}_x - \mathbf{u}^\dagger) + (\sigma(-p^\dagger,\mathbf{u}^\dagger)\mathbf{n} + (\mathbf{u}\cdot\mathbf{n})\mathbf{u}^\dagger)\delta\mathbf{g})\mathrm{d}\Gamma \\ & + \int_{\partial\Omega} (-\sigma(\delta p,\delta\mathbf{u})\mathbf{n}\cdot\mathbf{u}^\dagger + (\sigma(-p^\dagger,\mathbf{u}^\dagger)\mathbf{n} + (\mathbf{u}\cdot\mathbf{n})\mathbf{u}^\dagger)\delta\mathbf{u})\mathrm{d}\partial\Omega \\ & + \int_\Omega \{\nabla\cdot\mathbf{u}^\dagger\}\delta p\mathrm{d}\Omega \\ & - \int_\Omega ((-\mathbf{u}\cdot\nabla\mathbf{u}^\dagger + \mathbf{u}^\dagger\cdot\nabla\mathbf{u}^T - \nabla\cdot\sigma(-p^\dagger,\mathbf{u}^\dagger))\delta\mathbf{u} - \mathbf{u}^\dagger\delta\mathbf{f})\mathrm{d}\Omega,\end{aligned} \tag{A7}$$

since $\delta\mathbf{u} = \delta\mathbf{g}$ on Γ.

Grouping the terms multiplied by the flow variables, of the external force and the boundary condition perturbations:

$$\delta\mathscr{L} = \left\langle \frac{\partial\mathscr{L}}{\partial\mathbf{q}}, \delta\mathbf{q}\right\rangle_\Omega + \left\langle \frac{\partial\mathscr{L}}{\partial\mathbf{f}}, \delta\mathbf{f}\right\rangle_\Omega + \left\langle \frac{\partial\mathscr{L}}{\partial\mathbf{g}}, \delta\mathbf{g}\right\rangle_\Gamma. \tag{A8}$$

To obtain the adjoint equations, it is necessary to impose $\langle\frac{\partial\mathscr{L}}{\partial\mathbf{q}}, \delta\mathbf{q}\rangle_\Omega = 0$. Then, the governed equations for $(\mathbf{u}^\dagger, p^\dagger)$ with the boundary conditions can be written as

$$-\mathbf{u}\cdot\nabla\mathbf{u}^\dagger + \mathbf{u}^\dagger\cdot\nabla\mathbf{u}^T - \nabla\cdot\sigma(-p^\dagger,\mathbf{u}^\dagger) = \mathbf{f}, \tag{A9}$$

$$\nabla\cdot\mathbf{u}^\dagger = \mathbf{0}, \tag{A10}$$

$$\mathbf{u}^\dagger = (2,0) \quad \text{on } \Gamma, \tag{A11}$$

$$\mathbf{u}^\dagger = \mathbf{0} \quad \text{at inflow}, \tag{A12}$$

$$\mathbf{u}^\dagger = \mathbf{0} \quad \text{on walls}, \tag{A13}$$

$$\sigma(-p^\dagger,\mathbf{u}^\dagger)\mathbf{n} + (\mathbf{u}\cdot\mathbf{n})\cdot\mathbf{u}^\dagger = \mathbf{0} \quad \text{at outflow}. \tag{A14}$$

To get the sensitivity by an external force perturbation, $\delta\mathbf{g} = \mathbf{0}$ is imposed. Then, $\delta D = \delta\mathscr{L} = \langle\nabla_\mathbf{f} D, \delta\mathbf{f}\rangle_\Omega$, we get the following relation:

$$\nabla_{\mathbf{f}} D = \mathbf{u}^{\dagger}. \tag{A15}$$

Finally, we impose $\delta\mathbf{f} = \mathbf{0}$ to derive the sensitivity to a perturbation of the boundary body condition. So $\delta D = \delta\mathscr{L} = \langle \nabla_{\mathbf{g}} D, \delta\mathbf{g}\rangle_{\Gamma}$ and the relation ends as

$$\nabla_{\mathbf{g}} D = \sigma(-p^{\dagger}, \mathbf{u}^{\dagger})\mathbf{n} + (\mathbf{g}\cdot n)\mathbf{u}^{\dagger}. \tag{A16}$$

2. Sensitivity of aerodynamic drag for an unsteady flow

In this section, the quantity of interest is the mean aerodynamic drag coefficient around a body

$$\bar{D} = \frac{2}{T}\int_0^T \int_{\Gamma} \{\sigma(p,\mathbf{u})\mathbf{n}\cdot\mathbf{e}_x\} \mathrm{d}\Gamma \mathrm{d}t, \tag{A17}$$

where $(\mathbf{u}, p)$ is the solution in the domain, Ω, of unsteady incompressible Navier–Stokes equations

$$\frac{\partial u}{\partial t} + \mathbf{u}\cdot\nabla\mathbf{u} - \nabla\cdot\sigma(p,\mathbf{u}) = \mathbf{f}, \tag{A18}$$

$$\nabla\cdot\mathbf{u} = \mathbf{0}, \tag{A19}$$

with the following boundary conditions: $\mathbf{u} = \mathbf{g}$ on the body boundary, Γ, $\mathbf{u} = (1,0)$ on the upper and lower walls of the domain, $\mathbf{u} = (1,0)$ at the inflow, and $pn - \frac{1}{Re}\nabla\mathbf{u} = \mathbf{0}$ at the outflow.

For the derivation of the sensitivity in this regime, the Lagrangian is

$$\mathscr{L} = \bar{D} - \frac{1}{T}\int_0^T \int_{\Omega} \mathbf{u}^{\dagger}\cdot(\mathbf{u}\cdot\nabla\mathbf{u} - \nabla\cdot\sigma(p,\mathbf{u}) - \mathbf{f})\mathrm{d}\Omega\mathrm{d}t - \frac{1}{T}\int_0^T \int_{\Omega} p^{\dagger}\nabla\cdot\mathbf{u}\mathrm{d}\Omega\mathrm{d}t, \tag{A20}$$

where $\mathbf{q}^{\dagger} = (\mathbf{u}^{\dagger}, p^{\dagger})$ are the adjoint variables associated with the momentum equation and the conservation equation, respectively.

a. Adjoint equation for aerodynamics drag and sensitivities by an external force and by a perturbation of the body boundary condition. Introducing a perturbation on the force, $\mathbf{f} \to \mathbf{f} + \delta\mathbf{f}$, and a perturbation on the boundary condition, $\mathbf{g} \to \mathbf{g} + \delta\mathbf{g}$, the variation of the Lagrangian is defined as

$$\delta\mathscr{L} = \mathscr{L}(\mathbf{q} + \delta\mathbf{q}, \mathbf{q}^{\dagger}, \mathbf{f} + \delta\mathbf{f}) - \mathscr{L}(\mathbf{q}, \mathbf{q}^{\dagger}, \mathbf{f}). \tag{A21}$$

Using Eq. (A20) and Eq. (A17) into Eq. (A21) and developing it up to first order, we obtain the following expression:

$$\delta\mathscr{L} = \frac{2}{T}\int_0^T \int_{\Gamma} \{\sigma(\delta p, \delta\mathbf{u})\mathbf{n}\cdot\mathbf{e}_x\} d\Gamma - \frac{1}{T}\int_0^T \int_{\Omega} \mathbf{u}^{\dagger}\cdot(\delta\mathbf{u}\nabla\mathbf{u} + \mathbf{u}\nabla\delta\mathbf{u} - \nabla\cdot\sigma(\delta p, \delta\mathbf{u}) - \delta\mathbf{f})\mathrm{d}\Omega - \frac{1}{T}\int_0^T \int_{\Omega} p^{\dagger}\nabla\cdot\delta\mathbf{u}\mathrm{d}\Omega. \tag{A22}$$

Integrating by parts the previous equation and using the Green's first identity, we get

$$\begin{aligned}\delta\mathscr{L} = {} & \frac{1}{T}\int_0^T \int_{\Gamma} (\sigma(\delta p, \delta\mathbf{u})\mathbf{n}(2\mathbf{e}_x - \mathbf{u}^{\dagger}) + (\sigma(-p^{\dagger}, \mathbf{u}^{\dagger})\mathbf{n} \\ & + (\mathbf{u}\cdot\mathbf{n})\mathbf{u}^{\dagger})\delta\mathbf{g})\mathrm{d}\Gamma\mathrm{d}t + \frac{1}{T}\int_0^T \int_{\partial\Omega} (-\sigma(\delta p, \delta\mathbf{u})\mathbf{n}\cdot\mathbf{u}^{\dagger} \\ & + (\sigma(-p^{\dagger}, \mathbf{u}^{\dagger})\mathbf{n} + (\mathbf{u}\cdot\mathbf{n})\mathbf{u}^{\dagger})\delta\mathbf{u})\mathrm{d}\partial\Omega\mathrm{d}t \\ & + \frac{1}{T}\int_0^T \int_{\Omega} \{\nabla\cdot\mathbf{u}^{\dagger}\}\delta p\mathrm{d}\Omega\mathrm{d}t \\ & - \frac{1}{T}\int_0^T \int_{\Omega} \left(\left(-\frac{\partial\mathbf{u}^{\dagger}}{\partial t} - \mathbf{u}\cdot\nabla\mathbf{u}^{\dagger} + \mathbf{u}^{\dagger}\cdot\nabla\mathbf{u}^{T} \right. \right. \\ & \left. \left. -\nabla\cdot\sigma(-p^{\dagger}, \mathbf{u}^{\dagger}) \right)\delta\mathbf{u} \right)\mathrm{d}\Omega\mathrm{d}t + \frac{1}{T}\int_0^T \int_{\Omega} \mathbf{u}^{\dagger}\delta\mathbf{f}\mathrm{d}\Omega\mathrm{d}t \\ & - \frac{1}{T}\int_{\Omega} \mathbf{u}^{\dagger}\cdot\delta\mathbf{u}|_0^T \mathrm{d}\Omega. \end{aligned} \tag{A23}$$

Grouping the terms multiplied by the flow variables, the external force, and the boundary condition perturbations

$$\delta\mathscr{L} = \left\langle \frac{\partial\mathscr{L}}{\partial\mathbf{q}}, \delta\mathbf{q} \right\rangle_{\Omega,T} + \left\langle \frac{\partial\mathscr{L}}{\partial\mathbf{f}}, \delta\mathbf{f} \right\rangle_{\Omega,T} + \left\langle \frac{\partial\mathscr{L}}{\partial\mathbf{g}}, \delta\mathbf{g} \right\rangle_{\Gamma,T}. \tag{A24}$$

We impose $\langle \frac{\partial\mathscr{L}}{\partial\mathbf{q}}, \delta\mathbf{q}\rangle_{\Omega,T} = 0$ to obtain the adjoint equations. Then, the governed equations for $(\mathbf{u}^{\dagger}, p^{\dagger})$ can be written as

$$-\frac{\partial\mathbf{u}^{\dagger}}{\partial t} - \mathbf{u}\cdot\nabla\mathbf{u}^{\dagger} + \mathbf{u}^{\dagger}\cdot\nabla\mathbf{u}^{T} - \nabla\cdot\sigma(-p^{\dagger}, \mathbf{u}^{\dagger}) = \mathbf{f}, \tag{A25}$$

$$\nabla\cdot\mathbf{u}^{\dagger} = \mathbf{0}, \tag{A26}$$

with the following boundary and initial conditions:

$$\mathbf{u}^{\dagger} = (2,0) \quad \text{on } \Gamma, \tag{A27}$$

$$\mathbf{u}^{\dagger} = \mathbf{0} \quad \text{at inflow}, \tag{A28}$$

$$\mathbf{u}^{\dagger} = \mathbf{0} \quad \text{on walls}, \tag{A29}$$

$$\sigma(-p^{\dagger}, \mathbf{u}^{\dagger})\mathbf{n} + (\mathbf{u}\cdot n)\cdot\mathbf{u}^{\dagger} = \mathbf{0} \quad \text{at outflow}, \tag{A30}$$

$$\mathbf{u}^{\dagger}(T) = \mathbf{0}. \tag{A31}$$

To derive the sensitivity from an external force perturbation, $\delta\mathbf{g} = \mathbf{0}$ is imposed. Then, $\delta\bar{D} = \delta\mathscr{L} = \langle \nabla_{\mathbf{f}} D, \delta\mathbf{f}\rangle_{\Omega,T}$, and we reach the following relation:

$$\nabla_{\mathbf{f}} D = \mathbf{u}^{\dagger}. \tag{A32}$$

Finally, to obtain the sensitivity by a perturbation of the body boundary condition, $\delta\mathbf{f} = \mathbf{0}$ is imposed. Then, $\delta\bar{D} = \delta\mathscr{L} = \langle \nabla_{\mathbf{g}} D, \delta\mathbf{g}\rangle_{\Gamma,T}$, obtaining the following relation:

$$\nabla_{\mathbf{g}} D = \sigma(-p^{\dagger}, \mathbf{u}^{\dagger})\mathbf{n} + (\mathbf{g}\cdot n)\mathbf{u}^{\dagger}. \tag{A33}$$

3. Sensitivity of aerodynamic drag by a body geometry perturbation

For the calculation of the sensitivity to changes in geometry, we have used the previous calculation of the sensitivity to perturbations in the boundary condition with the perturbation obtained by the Theorem mentioned in Sec. II B, which gives us the relation between perturbation in the geometry and perturbation in the boundary condition,

$$\delta\mathbf{g} = -\frac{\partial \mathbf{u}}{\partial \mathbf{n}}(\delta\alpha \cdot \mathbf{n}), \tag{A34}$$

with $\delta\alpha = \Gamma - \Gamma_0$.

The important term in the analysis is, since it is the one that is multiplied by the perturbation in the boundary condition,

$$\frac{1}{T}\int_0^T \int_\Gamma (-\sigma(\delta p, \delta\mathbf{u})\mathbf{n}\cdot\mathbf{u}^\dagger + (\sigma(-p^\dagger, \mathbf{u}^\dagger)\mathbf{n} + (\mathbf{g}\cdot\mathbf{n})\mathbf{u}^\dagger)\delta\mathbf{g})\mathrm{d}\Gamma\mathrm{d}t = \left\langle \frac{\partial \mathscr{L}}{\partial \mathbf{g}}, \delta\mathbf{g}\right\rangle_{\Gamma,T}. \tag{A35}$$

By making the substitution Eq. (A34), we obtain

$$\nabla_\Gamma D = -\left(\sigma(-p^\dagger, \mathbf{u}^\dagger)\mathbf{n}\cdot\frac{\partial \mathbf{u}}{\partial \mathbf{n}}\right)\mathbf{n} - \left(\mathbf{u}^\dagger\cdot(\mathbf{g}\cdot\mathbf{n})\frac{\partial \mathbf{u}}{\partial \mathbf{n}}\right)\mathbf{n}. \tag{A36}$$

Note that we can use the aforementioned expression for the stationary case.

REFERENCES

[1]T. C. Corke and F. O. Thomas, "Active and passive turbulent boundary-layer drag reduction," AIAA J. **56**, 3835–3847 (2018).
[2]M. J. Walsh, "Riblets as a viscous drag reduction technique," AIAA J. **21**, 485–486 (1983).
[3]A. H. Duong, T. C. Corke, and F. O. Thomas, "Characteristics of drag-reduced turbulent boundary layers with pulsed-direct-current plasma actuation," J. Fluid Mech. **915**, A113 (2021).
[4]M. Gad-el Hak and R. F. Blackwelder, "Selective suction for controlling bursting events in a boundary layer," AIAA J. **27**, 308–314 (1989).
[5]M. Dhanak and C. Si, "On reduction of turbulent wall friction through spanwise wall oscillations," J. Fluid Mech. **383**, 175–195 (1999).
[6]P. Luchini and A. Bottaro, "Adjoint equations in stability analysis," Annu. Rev. Fluid Mech. **46**, 493–517 (2014).
[7]J. L. Lions, "*Optimal Control of Systems Governed by Partial Differential Equations*," (Springer, Berlin, 1971), Vol. 170.
[8]O. Pironneau, "On optimum design in fluid mechanics," J. Fluid Mech. **64**, 97–110 (1974).
[9]A. Jameson, "Aerodynamic design via control theory," J. Sci. Comput. **3**, 233–260 (1988).
[10]A. Jameson, "Optimum aerodynamic design using CFD and control theory," AIAA Paper No. 1995-1729, 1995.
[11]W. Huffman, R. Melvin, D. Young, F. Johnson, J. Bussoletti, M. Bieterman, and C. Hilmes, "Practical design and optimization in computational fluid dynamics," AIAA Paper No. 93-3111, 1993.
[12]J. Elliott and J. Peraire, "Practical three-dimensional aerodynamic design and optimization using unstructured meshes," AIAA J. **35**, 1479–1485 (1997).
[13]J. C. Newman III, A. C. Taylor III, R. W. Barnwell, P. A. Newman, and G. J.-W. Hou, "Overview of sensitivity analysis and shape optimization for complex aerodynamic configurations," J. Aircr. **36**, 87–96 (1999).
[14]M. B. Giles and N. A. Pierce, "An introduction to the adjoint approach to design," Flow, Turbul. Combust. **65**, 393–415 (2000).
[15]P. Meliga, E. Boujo, G. Pujals, and F. Gallaire, "Sensitivity of aerodynamic forces in laminar and turbulent flow past a square cylinder," Phys. Fluids **26**, 104101 (2014).
[16]A. Elham and M. J. van Tooren, "Discrete adjoint aerodynamic shape optimization using symbolic analysis with OpenFEMflow," Struct. Multidiscip. Optim. **63**, 2531–2551 (2021).
[17]A. Koreanschi, O. S. Gabor, J. Acotto, G. Brianchon, G. Portier, R. M. Botez, M. Mamou, and Y. Mebarki, "Optimization and design of an aircraft's morphing wing-tip demonstrator for drag reduction at low speeds, Part II—Experimental validation using infra-red transition measurement from wind tunnel tests," Chin. J. Aeronaut. **30**, 164–174 (2017).
[18]G. Molinari, A. F. Arrieta, and P. Ermanni, "Planform, aero-structural and flight control optimization for tailless morphing aircraft," J. Intell. Mater. Syst. Struct. **29**, 3847–3872 (2018).
[19]E. J. Nielsen and B. Diskin, "Discrete adjoint-based design for unsteady turbulent flows on dynamic overset unstructured grids," AIAA J. **51**, 1355–1373 (2013).
[20]W. Chen, C. Gao, Y. Gong, and W. Zhang, "Shape optimization to improve the transonic fluid-structure interaction stability by an aerodynamic unsteady adjoint method," Aerosp. Sci. Technol. **103**, 105871 (2020).
[21]G. K. Kenway, C. A. Mader, P. He, and J. R. Martins, "Effective adjoint approaches for computational fluid dynamics," Prog. Aerosp. Sci. **110**, 100542 (2019).
[22]C. A. Mader, J. R. Martins, J. J. Alonso, and E. Van Der Weide, "Adjoint: An approach for the rapid development of discrete adjoint solvers," AIAA J. **46**, 863–873 (2008).
[23]M. Chávez-Modena, L. M. González, and E. Valero, "Numerical optimization of the fin shape experiments of a heat conjugate problem surface air/oil heat exchanger (SACOC)," Int. J. Heat Mass Transfer **182**, 121971 (2022).
[24]M. D. Gunzburger, *Perspectives in Flow Control and Optimization* (SIAM, 2002).
[25]S. K. Nadarajah and A. Jameson, "Optimum shape design for unsteady flows with time-accurate continuous and discrete adjoint method," AIAA J. **45**, 1478–1491 (2007).
[26]O. Baysal and K. Ghayour, "Continuous adjoint sensitivities for optimization with general cost functionals on unstructured meshes," AIAA J. **39**, 48–55 (2001).
[27]J. Brezillon and N. Gauger, "2D and 3D aerodynamic shape optimisation using the adjoint approach," Aerosp. Sci. Technol. **8**, 715–727 (2004).
[28]K. Gkaragkounis, E. Papoutsis-Kiachagias, and K. Giannakoglou, "The continuous adjoint method for shape optimization in conjugate heat transfer problems with turbulent incompressible flows," Appl. Therm. Eng. **140**, 351–362 (2018).
[29]P. Meliga, E. Boujo, M. Meldi, and F. Gallaire, "Revisiting the drag reduction problem using adjoint-based distributed forcing of laminar and turbulent flows over a circular cylinder," Eur. J. Mech.-B/Fluids **72**, 123–134 (2018).
[30]J. Sokolowski and J.-P. Zolésio, "Introduction to shape optimization," in *Introduction to Shape Optimization* (Springer, 1992), pp. 5–12.
[31]M. Alnaes, J. Blechta, J. Hake, A. Johansson, B. Kehlet, A. Logg, C. Richardson, J. Ring, M. E. Rognes, and G. N. Wells, "The FEniCS project version 1.5," Archive Numer. Software **3**(100), 9–23 (2015).
[32]A. J. Chorin, "A numerical method for solving incompressible viscous flow problems," J. Comput. Phys. **135**, 118–125 (1997).
[33]J. P. Clark and E. A. Grover, "Assessing convergence in predictions of periodic-unsteady flowfields," J. Turbomach. **129**, 1831–1841 (2006).
[34]O. Posdziech and R. Grundmann, "A systematic approach to the numerical calculation of fundamental quantities of the two-dimensional flow over a circular cylinder," J. Fluids Struct. **23**, 479–499 (2007).
[35]S. Sen, S. Mittal, and G. Biswas, "Numerical simulation of steady flow past a circular cylinder," in Proceedings of the 37th National and 4th International Conference on Fluid Mechanics and Fluid Power, 2010, Vol. 16.
[36]Q. Wang and J.-H. Gao, "The drag-adjoint field of a circular cylinder wake at Reynolds numbers 20, 100 and 500," J. Fluid Mech. **730**, 145–161 (2013).
[37]A. Martinez-Cava, M. Chávez-Modena, E. Valero, J. de Vicente, and E. Ferrer, "Sensitivity gradients of surface geometry modifications based on stability analysis of compressible flows," Phys. Rev. Fluids **5**, 063902 (2020).
[38]J. Brewster and M. P. Juniper, "Shape sensitivity of eigenvalues in hydrodynamic stability, with physical interpretation for the flow around a cylinder," Eur. J. Mech.-B/Fluids **80**, 80–91 (2020).